The Study of a Phosphate Conversion Coating on Magnesium Alloy AZ91D: I. Formation, Morphology and Composition

Yong Zhou, Qing yun Xiong, Jin ping Xiong[*]

Beijing Key Laboratory of Electrochemical Process and Technology for Materials,
Beijing University of Chemical Technology, Beijing 100029, China
Key Laboratory of Carbon Fiber and Functional Polymer of Education Ministry,
Beijing University of Chemical Technology, Beijing 100029, China
[*]E-mail: xiongjp@mail.buct.edu.cn

This paper involved a phosphate conversion coating on magnesium alloy AZ91D. The formation of the phosphate conversion coating was studied with potential-time curve and electrochemical impedance spectroscopy (EIS), and the morphology and composition of the phosphate conversion coating were analyzed with scanning electron microscope (SEM), X-ray diffraction (XRD) and X-ray photoelectron spectroscopy (XPS). The results showed that the growth process of the phosphate conversion coating could be divided into three steps. In the first step (0-40 s) the potential fluctuated sharply due to the alternate presence and absence of the metastable crystal nucleuses and the formation of the stable crystal nucleuses composed of the elements of Zn, P and O. In the second step (40-200 s) the potential moved to the negative direction because of the electrochemical inhomogeneity attributed to the growth of the stable crystal nucleuses until the magnesium alloy surface was covered by the slab-like phosphate crystals completely. In the finally step (200-1200 s) the potential move to the positive direction slowly until it leveled off because the thickness of the phosphate conversion coating increased gradually from the slab-like phosphate crystals initially. The magnesium alloy substrate was isolated from the acidic and corrosive phosphating bath by the phosphate conversion coating, which was formed completely at 1200s. The phosphate conversion coating showed a uniform, compact and integral crystal clusters and was composed of $Zn_3(PO_4)_2$, $Zn_2Mg(PO_4)_2$ and Zn.

1. INTRODUCTION

Magnesium alloys have many good performances: low density, high thermal conductivity, good electromagnetic features, high strength to weight ratio and good recyclability [1]. However, the natural oxide film on magnesium alloys surface is porous and cannot provide good protection for

magnesium alloys substrate [2], resulting that the corrosion susceptibility of magnesium alloys is higher than that of other alloys, which limits the wide application of magnesium alloys [3]. Phosphate conversion coatings are one of the common surface protective methods to strengthen the corrosion resistance of magnesium alloys, which have some advantages such as easy operation, low cost and little size limitation [4].

At present, phosphate conversion coatings on magnesium alloys have been studied widely, which mainly focus on the preparation and protection of phosphate conversion coatings. Lian et al. [5] prepared a zinc phosphate conversion coating on magnesium alloy AZ91D in a phosphating bath containing H_3PO_4, ZnO and NaF mainly. The zinc phosphate conversion coating had typical phosphate microstructure, and the composition analyzed by XRD were $Zn_3(PO_4)_2 \cdot 4H_2O$, Zn, $AlPO_4$ and $Zn_2Mg(PO_4)_2$. SEM had shown that very fine zinc particles surrounded phosphate crystals and filled in the interstice of the insoluble phosphate. Liu et al. [6] prepared a new molybdate-phosphate conversion coating on magnesium alloy AM60. The molybdate-phosphate coating contained composite phases, which were consisted of metaphosphate as well as molybdate oxide with an "alveolate-crystallized" structure. The composite coating had better corrosion resistance performance than molybdate coating, and even had almost comparable corrosion protection for the magnesium alloy to the traditional chromate-based coating. Zeng et al. [7] prepared a zinc phosphate conversion coating and a zinc-calcium phosphate conversion coating on magnesium alloy AZ31D. The flowerlike zinc-calcium coating was mainly composed of $Zn_3(PO_4)_2 \cdot 4H_2O$. They had a quite different morphology from the dry-revered-like zinc coating that consisted of MgO, MgF_2, Zn and $Zn_3(PO_4)_2 \cdot 4H_2O$. Both of the zinc and zinc-calcium coating could remarkably reduce the corrosion current density of the magnesium alloy substrate. The zinc-calcium coating showed better corrosion resistance than the zinc coating.

However, the studies involving the formation of phosphate conversion coatings on magnesium alloys are relatively less [8,9]. In this paper, the formation of a phosphate conversion coating on magnesium alloy AZ91D was studied with potential-time curve, scanning electron microscope (SEM) and electrochemical impedance spectroscopy (EIS), and the composition of the phosphate conversion coating was analyzed with X-ray diffraction (XRD) and X-ray photoelectron spectroscopy (XPS).

2. EXPERIMENTAL

2.1 Material and preparation

The studied material was magnesium alloy AZ91D with following chemical composition (wt%): Al, 9.4; Zn, 0.82; Mn, 0.23; Si, 0.01; Cu, 0.02; Ni 0.0021; Fe, 0.005, and Mg. Samples were manually abraded up to 1000 grit with SiC abrasive, rinsed with de-ionized water and degreased in alcohol. The surface area of the magnesium alloy samples for electrochemical measures was 1.0 cm^2, and the dimensions of the magnesium alloy samples for SEM, XRD and XPS analyses was 25 mm × 15 mm × 5 mm.

2.2 Preparation of the phosphate conversion coating on the magnesium alloy sample

The phosphate conversion coating was formed on the sample surface at 45 ℃ by immersing the sample into the phosphating bath with the composition as follows: ZnO, 2.0 g/L; H_3PO_4, 12.0 g/L; NaF, 1.0 g/L; $C_4H_6O_6Na_2$, 4.0 g/L; $NaNO_3$, 6.0 g/L; $Na_4P_2O_7$, 0.5 g/L.

2.3 Electrochemical measuremnts

The potential-time curve was carried out using a CS350 electrochemical workstation (China) in the phosphating bath, and the potential recording frequency was 5 Hz. In this test, the working electrode was a magnesium alloy sample with 1.0 cm^2 exposed to the phosphating bath, and the reference electrode was a saturated calomel electrode (SCE). EIS plots were performed using a Princeton 2273 instrument (USA). During the EIS test, a perturbation potential of 10 mV amplitude was applied with the frequency range from 10^5 to 10^{-2} Hz. A typical three electrode system was used for the EIS test. The system was composed of a saturated calomel electrode (SCE) as reference electrode, a platinum sheet as counter electrode, and the magnesium alloy sample with 1.0 cm^2 as working electrode exposed to 3.5 % (wt%) NaCl solution. The test temperatures of the potential-time curve and the EIS plots were 45 ℃ and 25 ℃, respectively.

2.4 Scanning electron microscope (SEM) observation

The surface morphology of the magnesium alloy samples was observed with a LEO-1450 SEM (USA).

2.5 X-ray diffraction (XRD) and X-ray photoelectron spectroscopy (XPS) analysis

The surface composition of the magnesium alloy samples was analyzed with a 2500VB2+PC XRD (Japan) and an ESCALAB-250 XPS (USA).

3. RESULTS AND DISCISSION

3.1 Potential-time curve test

The potential of magnesium alloy AZ91D immersed in the phosphating bath at 45 ℃ was recorded with time, as showed in Fig. 1. The potential-time curve can be divided into three steps. In the first step (0-40 s) the potential fluctuates seriously, and the values of potential peak and potential valley are -0.586 V_{SCE} and -0.604 V_{SCE}, respectively. In the second step (40-200 s) the potential moved to the negative direction until the minimum value of potential is reached about -0.612 V_{SCE}. In the finally step (200-2000 s) the potential move to the positive direction slowly until it leveled off about -0.548 V_{SCE}.
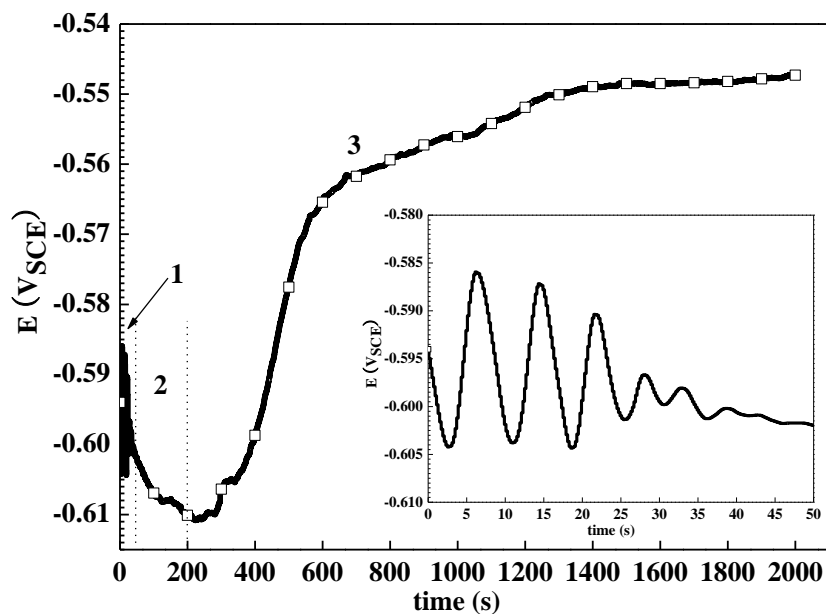
Figure 1. Potential-time curve of magnesium alloy AZ91D immersed in the phosphating bath at 45 ℃.

3.2 SEM observations
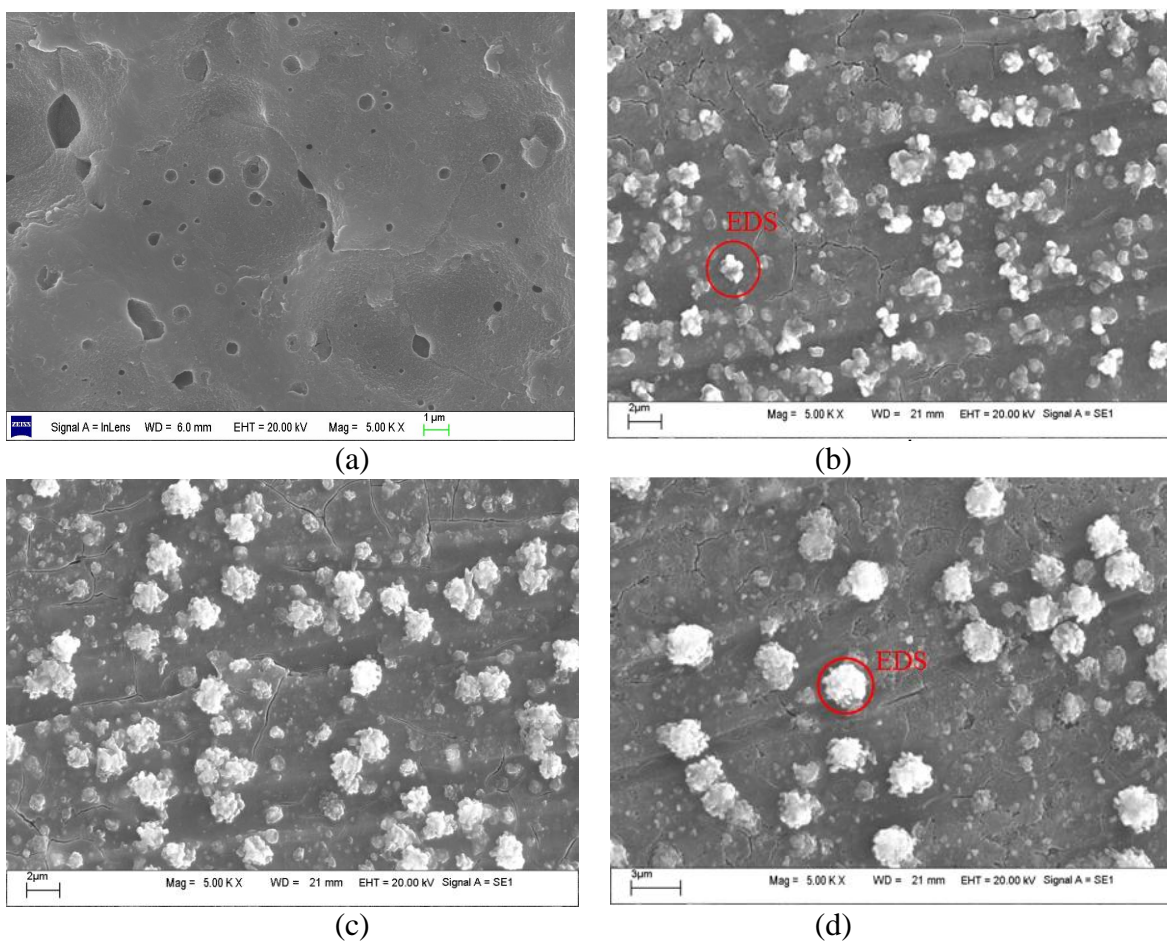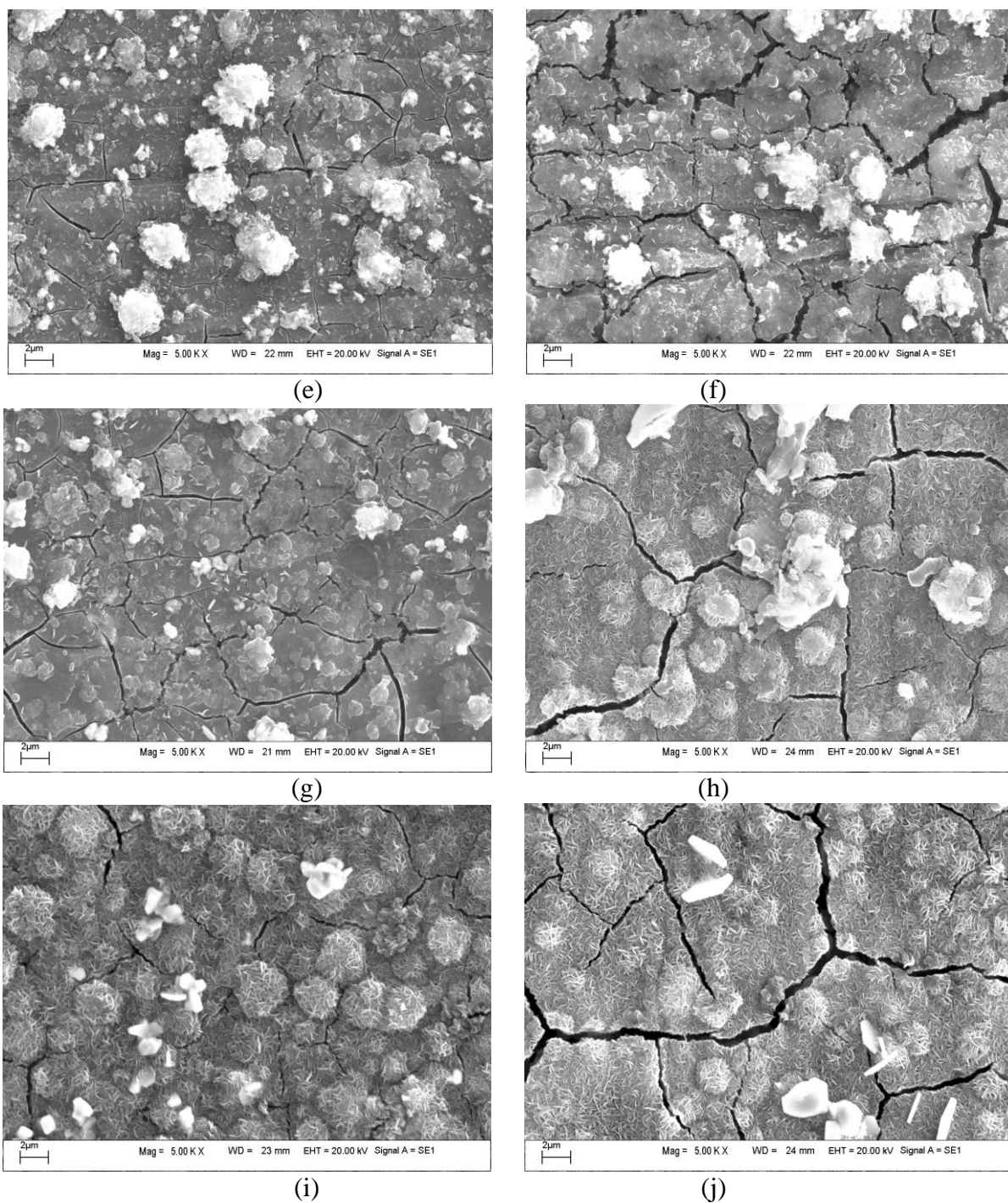
Figure 2. Surface SEM morphologies of the magnesium alloy sample immersed in the phosphating bath with different time: (a) 0 s, (b) 10 s, (c) 30 s, (d) 40 s, (e) 100 s, (f) 200 s, (g) 5 min, (h) 10 min, (i) 20 min and (j) 30 min.

Fig. 2 shows the surface SEM morphologies of the magnesium alloy AZ91D samples immersed in the phosphating bath at 45 ℃ for different time. Fig. 2a shows the surface SEM morphology of the sample without immersion in the phosphating bath. There is an air-formed and multi-porous film on the sample surface, and EDS analysis revealed that Mg and O were present in the film. Song et al. [3,4] reported that the natural passive film on magnesium alloys surface was

composed of MgO and $Mg(OH)_2$, and the EDS result is consistent with Song et al.'s studies. Fig. 2b shows the surface SEM morphology of the sample immersed in the phosphating bath for 10 s. Many "white flowers" structures can be observed, and EDS analysis revealed that the elements of Zn, P and O were present in the "white flowers" structure marked by red circle in Fig. 2b, indicating that "white flowers" structures may be the metastable crystal nucleuses of $Zn_3(PO_4)_2$. From Fig. 2b, many small metastable crystal nucleuses form uniformly on the sample surface, which has an average size of 1-2 μm. There are about 2.0×10^4 crystal nucleuses calculated per square centimeter. Such a great number of metastable crystal nucleuses distributed equably on the sample surface indicates that the formation of the phosphate conversion coating should occur uniformly on each phases of magnesium alloy AZ91D. Fig. 2c and 2d show the surface SEM morphologies of the sample immersed in the phosphating bath for 30 s and 40 s. From 10 s to 40 s the quantity of crystal nucleuses decrease, but the bulk of crystal nucleuses increase. During this period (10-40 s) only a small amount of metastable crystal nucleuses grow up or join together to form some bigger "white flowers" structure with the size about 3-5 μm, and EDS analysis revealed that the relative atom ratios of Zn, P and O were approximately 3 : 2 : 8, indicating the stable crystal nucleuses of $Zn_3(PO_4)_2$. However, a majority of metastable crystal nucleuses cannot grow and disappear at last. The alternate presence and absence of the metastable crystal nucleuses on the sample surface caused the potential fluctuated in the period of 0-40 s, as showed in the embedded figure in Fig. 1. Fig. 2e and 2f show the surface SEM morphologies of the sample immersed in the phosphating bath for 100 s and 200 s. The stable crystal nucleuses grow gradually, and the slab-like phosphate crystals with cracks and porous can be observed on the sample surface when the immersion time is 200 s. The electrochemical homogeneity of the magnesium alloy surface was damaged during the growth process from stable crystal nucleuses to slab-like phosphate crystals, which leaded to the negative movement of potential. Fig. 2g shows the surface SEM morphology of the sample immersed in the phosphating bath for 5 min. The sample surface was fully covered by the phosphate conversion coating, but there are some cracks observed as the result of the hydrogen evolution reaction. With the increase of immersion time, from Fig. 2h and 2i the width of cracks decreases gradually with the immersion time in the range from 10 min to 20 min. Fig. 2i shows the surface SEM morphology of the sample immersed in the phosphating bath for 20 min. The width of cracks is least, and the phosphate conversion coating shows a uniform, compact and integral crystal clusters structure. However, the surface SEM morphology of the phosphate conversion coating with the immersion time of 30 min is similar to that with the immersion time of 10 min, as showed in Fig. 2j. The reason may be as follows: the phosphate conversion coating has been formed completely when the immersion time is 20 min, after that, the coating was dissolved partly in the acidic and corrosive phosphating bath. The thickness of the phosphate conversion coating increased gradually from the slab-like phosphate crystals initially until the phosphate conversion coating formed completely, which lead to the positive movement of potential.

3.3 EIS plots

Fig. 3 shows the Nyquist plots of the naked magnesium alloy and the phosphated magnesium alloys immersed in the phosphating bath for different time. The Nyquist plots of the naked magnesium

alloy and the phosphated magnesium alloys with the immersion time of 10 s, 30 s, 100 s and 200 s are composed of a capacitive loop at high frequency and an inductive loop at low frequency.
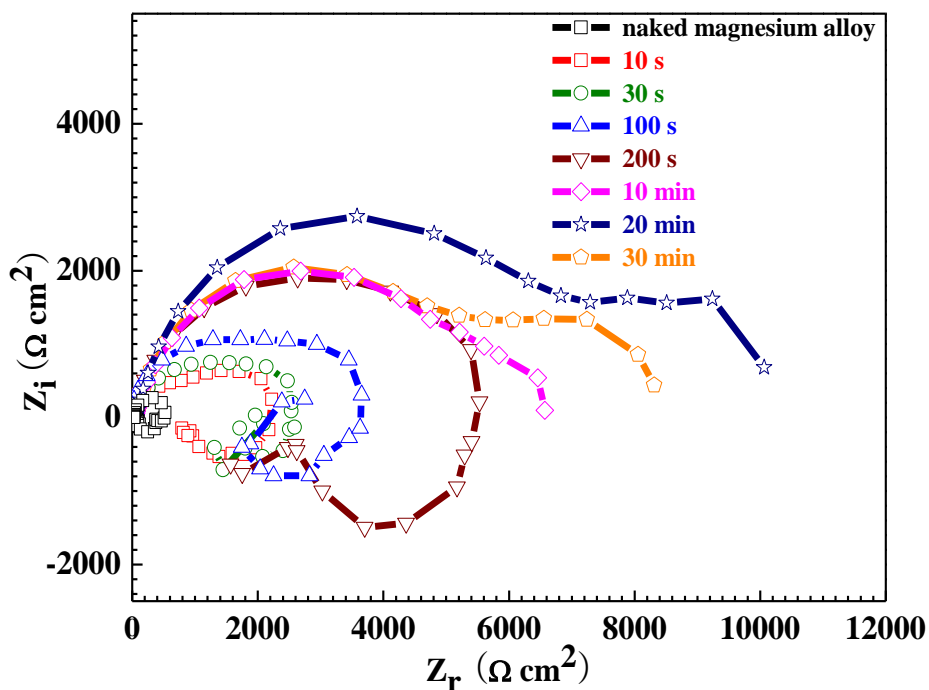
Figure 3. Nyquist plots of the naked magnesium alloy and the phosphated magnesium alloys immersed in the phosphating bath with different time.

The capacitive loops at high frequency reflect the electrochemical impedance characteristics of a film and the double electron layer on the metals surface [6], and the inductive loops at low frequency are attributed to the occurrence of pitting corrosion [10] or the adsorption relaxation process of some species such as intermediates [11], organic inhibitors [12], anions and cations [13] or gas molecules [14]. In contrast, the Nyquist plots of the phosphated magnesium alloys with the immersion time of 10 min, 20 min and 30 min are composed of an enlarged capacitive loop at high and intermediate frequency and a depressed capacitive loop at low frequency. The capacitive loops at high and intermediate frequency reflect the electrochemical impedance characteristics of the double electron layer and the charge transfer process [15], and the capacitive loops at low frequency are attributed the presence of a protective film, the phosphate conversion film here. When the immersion time reaches 10 min, as showed in Fig. 3, the separation of the capacitive loops and the absence of the inductive loops may be attributed to the complete cover of the phosphate conversion coating on the magnesium alloy surface. However, the radius of the capacitive loop of the phosphated magnesium alloy immersed for 10 min is smaller than that of the phosphated magnesium alloy immersed for 20 min, indicating that the thickness of the phosphate conversion coating grown for 20 min is thicker than that grown for 10 min. The radius of the capacitive loop of the phosphated magnesium alloy immersed for 30 min is also smaller than that of the phosphated magnesium alloy immersed for 20 min, which is attributed to the localized dissolution of the phosphate conversion coating in the acidic and corrosive phosphating

bath consistent with the SEM results showed in Fig. 2i and 2j. Further, inductive loops can be observed with immersion time of 10 s, 30 s, 100 s and 200 s, which is attributed the occurrence of pitting corrosion induced by chloride anions in NaCl solution because the magnesium alloy surface cannot be covered by the phosphate conversion coating completely at this time. The similar result was reported by Cheng et al. [16] that there would be an inductive loop in the low frequency region of EIS.

However, the radius of capacitive loops of the phosphated magnesium alloys is larger than that of the naked magnesium alloy, indicating that the phosphate conversion coating provided a degree of protection for the magnesium alloy substrate.

From the above results, the formation of the phosphate conversion coating can be divided three steps: 0-40 s, 40-200 s and 200 s-20 min. The electrode potential, SEM morphology and impedance are closely related with the immersion time, and the phosphate conversion coating shows compact and integral structure and provides good protection for the magnesium alloy substrate when the immersion time is 20 min.

3.4 XRD analysis
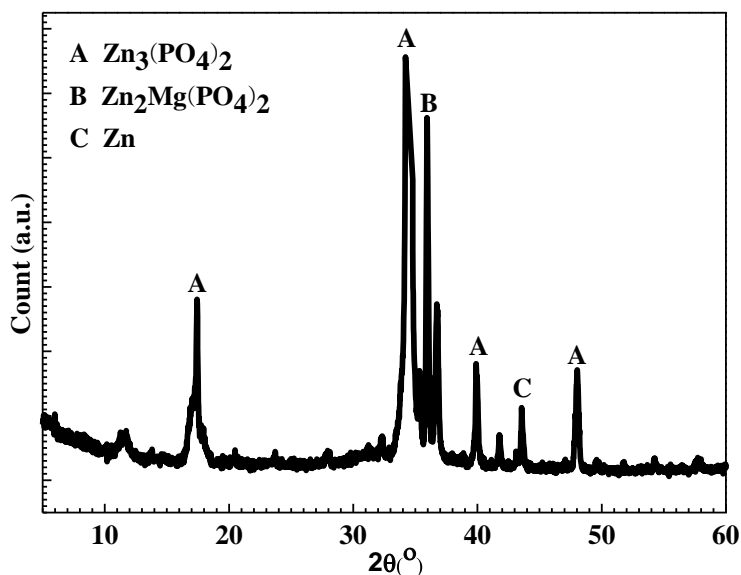
Figure 4. XRD spectrum of the phosphate conversion coating formed in the phosphating bath at 45 ℃ for 20 min.

Fig. 4 shows the XRD spectrum of the phosphate conversion coating formed in the phosphating bath at 45 ℃ for 20 min. The major phases of the phosphate conversion coating are composed of $Zn_3(PO_4)_2$, $Zn_2Mg(PO_4)_2$ and Zn. The XRD result is consistent with the studies of Li et al. [17] and Liu et al. [6].

3.5 XPS analysis
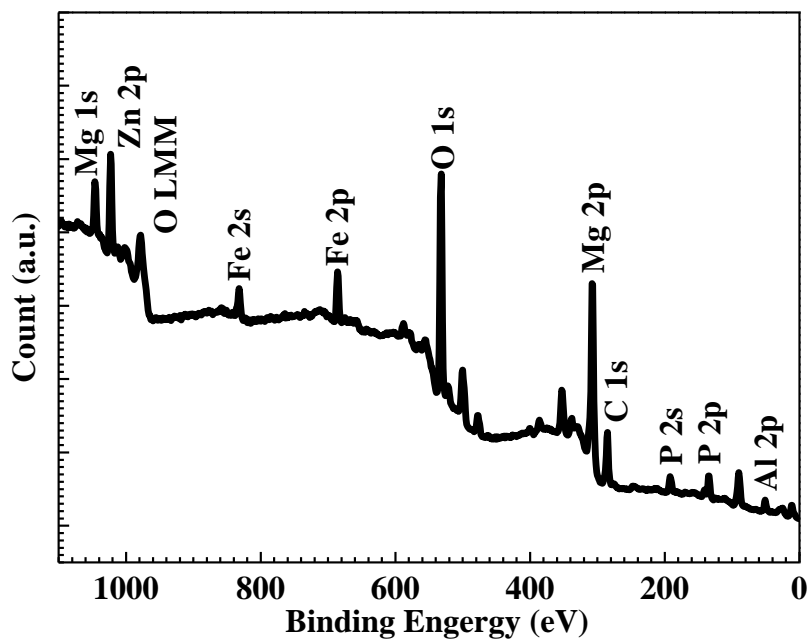
Figure 5. Wide-scan XPS spectrum of the phosphate conversion coating formed in the phosphating bath at 45 ℃ for 20 min.
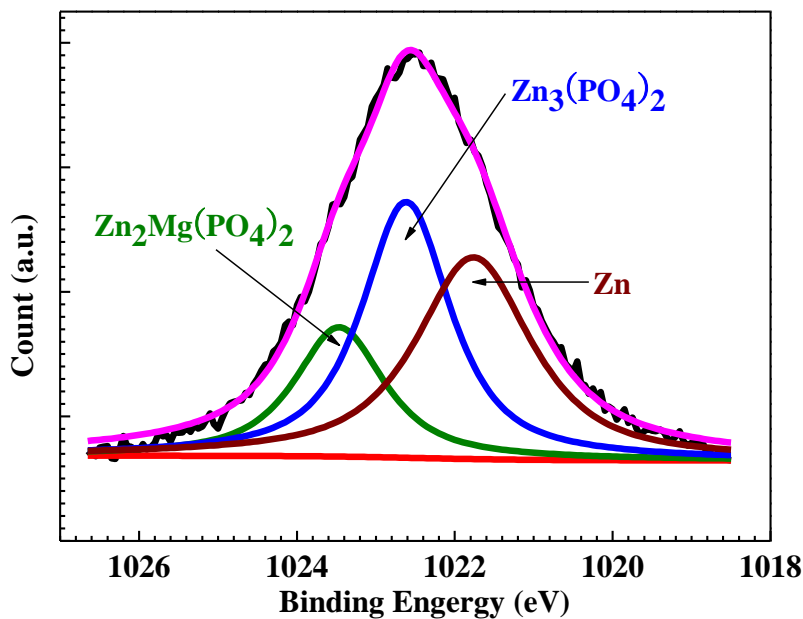
Figure 6. High-resolution XPS spectrum of Zn 2p of the phosphate conversion coating formed in the phosphating bath at 45 ℃ for 20 min.

Fig. 5 shows the wide-scan XPS spectrum of the phosphate conversion coating formed in the phosphating bath at 45 ℃ for 20 min. The XPS results provide evidence for the presence of Mg, Zn, Fe, O, C, P and Al, consistent with the EDS result. Fig. 6 shows the high-resolution XPS spectrum of Zn 2p of the phosphate conversion coating. The Zn 2p spectrum reveals three peaks at 1023.50 eV, 1022.60 eV and 1021.75 eV, which correspond to Zn element in $Zn_2Mg(PO_4)_2$, $Zn_3(PO_4)_2$ and Zn, respectively.
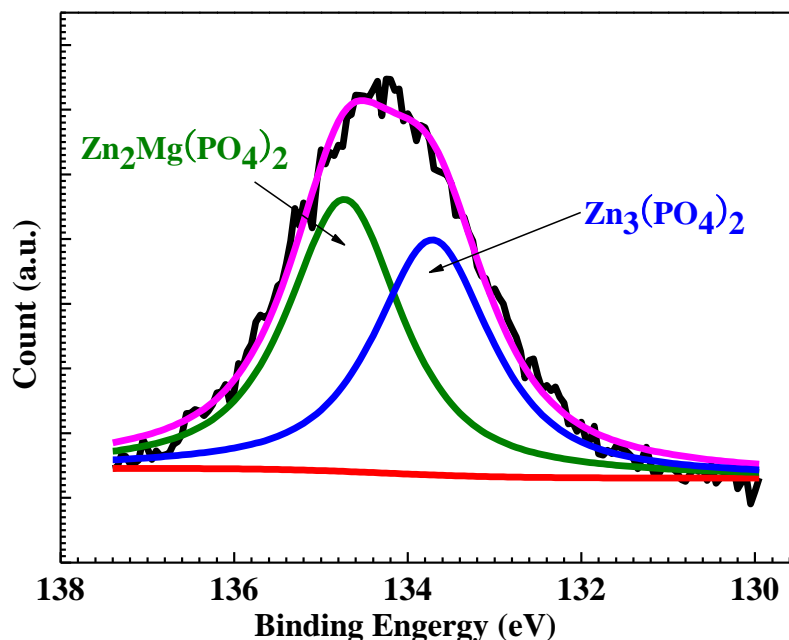
Figure 7. High-resolution XPS spectrum of P 2p of the phosphate conversion coating formed in the phosphating bath at 45 ℃ for 20 min.

Fig. 7 shows the high-resolution XPS spectrum of P 2p of the phosphate conversion coating. The P 2p spectrum reveals two peaks at 134.75 eV and 133.70 eV, corresponding to P element in $Zn_2Mg(PO_4)_2$ and $Zn_3(PO_4)_2$, respectively. Fig. 8 shows the high-resolution XPS spectrum of O 1s of the phosphate conversion coating. The O 1s spectrum reveals three peaks at 532.90 eV, 531.95 eV and 531.00 eV, corresponding to O element in $Zn_2Mg(PO_4)_2$, $Zn_3(PO_4)_2$ and H_2O, respectively. $Zn_2Mg(PO_4)_2$ and $Zn_3(PO_4)_2$ is the main component of the phosphate conversion coatings on magnesium alloy AZ91D, which is consistent with the studies from Li et al. [17] and Niu et al. [18].

The above XPS results are consistent with the XRD results showed in Fig. 4, indicating that the phosphate conversion coating is composed of $Zn_3(PO_4)_2$, $Zn_2Mg(PO_4)_2$ and Zn. The formation of the phosphate conversion coating on magnesium alloy AZ91D may be as follows. When the magnesium alloy sample was immersed in the acidic phosphating bath, the reaction (1) occurred in the magnesium alloy surface, resulting that the value of pH increased and the concentration of H^+ decreased near the magnesium alloy surface:

$$Mg + 2H^+ \longrightarrow Mg^{2+} + H_2 \quad (1)$$
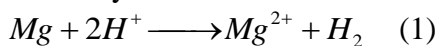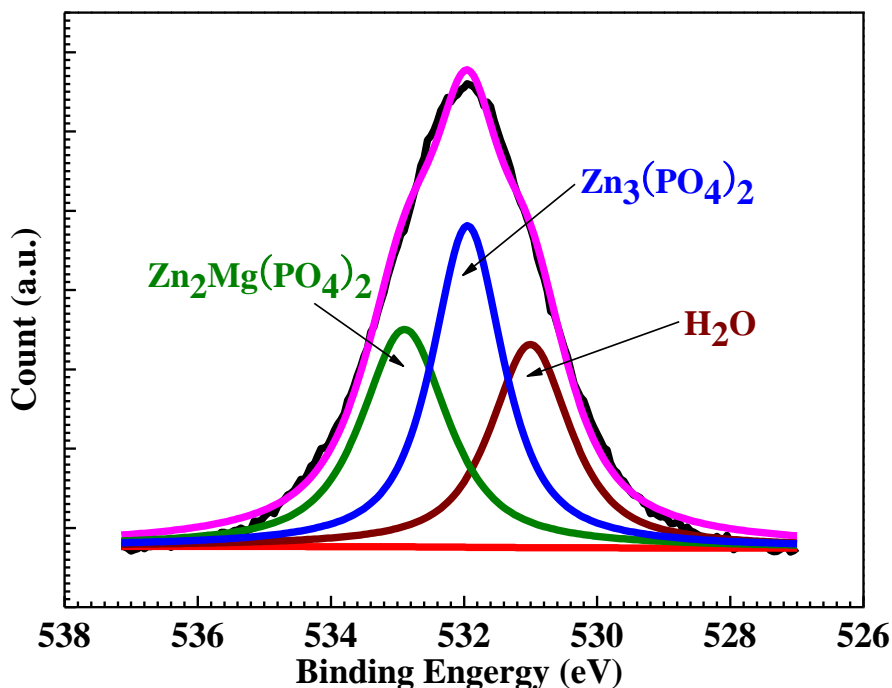
Figure 8. High-resolution XPS spectrum of O 1s of the phosphate conversion coating formed in the phosphating bath at 45 ℃ for 20 min.

The increase of pH value and the decrease of H^+ concentration caused the equilibrium of reaction (2), (3) and (4) to move the right direction:

$$ZnO + 2H_3PO_4 + H_2O \longrightarrow Zn(H_2PO_4)_2 \cdot 2H_2O \quad (2)$$

$$Zn(H_2PO_4)_2 \cdot 2H_2O \longrightarrow ZnPO_4^- + H_2PO_4^- + 2H^+ + 2H_2O \quad (3)$$

$$ZnPO_4^- \longrightarrow Zn^{2+} + PO_4^{3-} \quad (4)$$
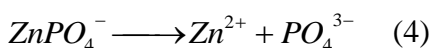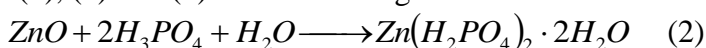
Therefore, Zn^{2+}, $H_2PO_4^-$ and PO_4^{3-} were enriched and reached supersaturation near the magnesium alloy surface. However, when the concentrations of Zn^{2+}, $H_2PO_4^-$ and PO_4^{3-} were higher than the solubility products of $Zn_3(PO_4)_2$ and $Zn_2Mg(PO_4)_2$, the following reaction (5), (6), (7) and (8) could occur and the phosphate conversion coating formed on the magnesium alloy surface:

$$3Zn^{2+} + 2PO_4^{3-} + 4H_2O \longrightarrow Zn_3(PO_4)_2 \cdot 4H_2O \quad (5)$$

$$2Zn^{2+} + Mg^{2+} + 2PO_4^{3-} + 4H_2O \longrightarrow Zn_2Mg(PO_4)_2 \cdot 4H_2O \quad (6)$$

$$3Zn^{2+} + 2H_2PO_4^- + 4H_2O + 4e^- \longrightarrow Zn_3(PO_4)_2 \cdot 4H_2O + 2H_2 \quad (7)$$

$$2Zn^{2+} + Mg^{2+} + 2H_2PO_4^- + 4H_2O + 4e^- \longrightarrow Zn_2Mg(PO_4)_2 \cdot 4H_2O + 2H_2 \quad (8)$$
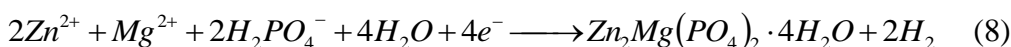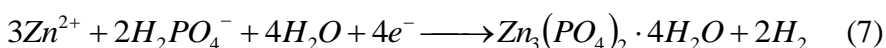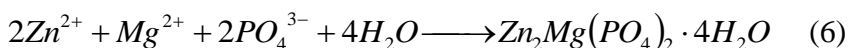
On the other hand, the formation of the phosphate conversion coating caused the consumption of Zn^{2+}, $H_2PO_4^-$ and PO_4^{3-}, further resulting in the right direction move of reaction (2), (3) and (4) and a new equilibrium was reached. At the same time, because the redox potential of Zn was higher than that of Mg [19,20], the generated Zn^{2+} by reaction 4 could get the electrons derived from the oxidation of Mg as follows:

$$Zn^{2+} + 2e^- \longrightarrow Zn \quad (9)$$

Therefore, the presence of Zn can be detected by XRD and XPS, as showed in Fig. 4 and Fig. 5.

4. CONCLUSIONS

(1) The growth process of the phosphate conversion coating on magnesium alloy AZ91D could be divided into three steps. In the first step (0-40 s) the potential fluctuated sharply due to the alternate presence and absence of the metastable crystal nucleuses and the formation of the stable crystal nucleuses. In the second step (40-200 s) the potential moved to the negative direction because of the electrochemical inhomogeneity attributed to the growth of the stable crystal nucleuses. In the finally step (200-1200 s) the potential move to the positive direction slowly until it leveled off because the thickness of the phosphate conversion coating increased gradually from the slab-like phosphate crystals initially.

(2) The phosphate conversion coating showed a uniform, compact and integral crystal clusters and was composed of $Zn_3(PO_4)_2$, $Zn_2Mg(PO_4)_2$ and Zn.

References

1. J.E. Gray and B. Luan, *Journal of Alloys and Compounds*, 336 (2002) 88.
2. T.S. Shih, J.B. Liu and P.S. Wei, *Materials Chemistry and Physics*, 104 (2007) 497.
3. G.L. Song and D.S. John, *Corrosion Science*, 46 (2004) 1381.
4. G.L. Song and D.S. John, *Materials and Corrosion*, 56 (2005) 15.
5. L.Y. Niu, Z.H. Jiang, G.Y. Li, C.D. Gu and J.S. Lian, *Surface & Coating Technology*, 200 (2006) 3021.
6. Z.Y. Yong, J. Zhu, C. Qiu and Y.L. Liu, *Applied Surface Science*, 255 (2008) 1672.
7. R.C. Zeng, Z.D. Lan, L.H. Kong, Y.D. Huang and H.Z. Cui, *Surface & Coating Technology*, 205 (2011) 3347.
8. G.Y. Li, J.S. Lian, L.Y. Niu, Z.H. Jiang and Q. Jiang, *Surface & Coating Technology*, 201 (2006) 1814.
9. L. Kouisni, M. Azzi, M. Zertoubi, F. Dalard and S. Maximovitch, *Surface & Coating Technology*, 185 (200) 58.
10. J.L. Poli, E. Cano and J.M. Bastidas, *Journal of Electroanalytical Chemistry*, 537 (2002) 183.
11. 11 L. Benea, P.L. Bonora, A. Borello, S. Martelli, F. Wenger, P. Ponthiaux and J. Galland, *Solid State Ionics*, 151 (2002) 89.
12. S.A. Umoren, Y. Li and F.H. Wang, *Corrosion Science*, 52 (2010) 2422.
13. K.F. Khaled, *Corrosion Science*, 52 (2010) 2905.
14. N. Wager and E. Gulzow, *Journal of Power Sources*, 127 (2004) 341.
15. H.P. Duan, K.Q. Du, C.W. Yan and F.H. Wang, *Electrochimica Acta*, 51 (2006) 2898.
16. Y.L. Cheng, H.L. Wu, Z.H. Chen, H.M. Wang, Z. Zhang and Y.W. Wu, *Transactions of Nonferrous Metals Society of China*, 17 (2007) 502.
17. Q. Li, S.Q. Xu, J.Y. Hu, S.Y. Zhang, X.K. Zhong and X.K. Yang, *Electrochimica Acta*, 55 (2010) 887.

18. L.Y. Niu, J.X. Lin, Y. Li, Z.M. Shi and L.C. Xu, *Transactions of Nonferrous Metals Society of China*, 20 (2010) 1356.
19. J. Park and C.K. Lee, *Surface & Coating Technology*, 259 (2014) 50.
20. Z.P. Xie, Q.C. Liu, Z.W. Chang and X.B. Zhang, *Electrochimica Acta*, 90 (2013) 695.